Electrochemical and Structural Properties of $xLi_2M'O_3\cdot(1-x)LiMn_{0.5}Ni_{0.5}O_2$ Electrodes for Lithium Batteries (M′ = Ti, Mn, Zr; $0 \leq x \leqslant 0.3$)

Jeom-Soo Kim, Christopher S. Johnson, John T. Vaughey, and Michael M. Thackeray*

Electrochemical Technology Program, Chemical Engineering Division, Argonne National Laboratory, Argonne, Illinois 60439

Stephen A. Hackney

Department of Metallurgical and Materials Engineering, Michigan Technological University, Houghton, Michigan 49931

Wonsub Yoon

Brookhaven National Laboratory, Upton, New York 11973

Clare P. Grey

Department of Chemistry, State University of New York, Stony Brook, New York 11794

Received December 24, 2003. Revised Manuscript Received March 4, 2004

Electrochemical and structural properties of $xLi_2M'O_3\cdot(1-x)LiMn_{0.5}Ni_{0.5}O_2$ electrodes (M′ = Ti, Mn, Zr; $0 \leq x \leq 0.3$) for lithium batteries are reported. Powder X-ray diffraction, lattice imaging by transmission electron microscopy, and nuclear magnetic resonance spectroscopy provide evidence that, for M′ = Ti and Mn, the $Li_2M'O_3$ component is structurally integrated into the $LiMn_{0.5}Ni_{0.5}O_2$ component to yield "composite" structures with domains having short-range order, rather than true solid solutions in which the cations are uniformly distributed within discrete layers. Li_2TiO_3 and Li_2ZrO_3 components are electrochemically inactive, whereas electrochemical activity can be induced into the Li_2MnO_3 component above 4.3 V vs Li^0. When cycled in lithium cells, $xLi_2MnO_3\cdot(1-x)LiMn_{0.5}Ni_{0.5}O_2$ electrodes with $x = 0.3$ provide capacities in excess of 300 mA·h/g over the range 4.6−1.45 V.

Introduction

Layered lithium transition-metal-oxide electrodes Li_xMO_2 (M = Co, Ni, and Mn) become unstable at low lithium content when lithium cells are charged above 4.3 V. At this potential, the oxygen activity at the electrode surface is increased to a level at which side reactions can occur, such as electrolyte oxidation or oxygen loss. For several years, following the discovery that acid treatment of Li_2MnO_3 produces a novel layered $Li_{2-x}MnO_{3-x/2}$ structure,[1] which on relithiation yields a compound that can be formulated as $xLi_2M'O_3\cdot(1-x)LiMO_2$[2] (ignoring the H^+ ion exchange that occurs during acid treatment),[1,3] we have pursued an approach using an electrochemically inactive $Li_2M'O_3$ component (e.g., Mn, Ti, or Zr) to stabilize these layered $LiMO_2$ structures. In particular, we have used this approach in attempts to prevent the conversion of layered $LiMnO_2$ to spinel.[4,5] Our efforts to stabilize layered $LiMn_{1-x}Ni_xO_2$ electrodes followed reports by Pacific Lithium Ltd. that $Li_{1.2}Mn_{0.4}Cr_{0.4}O_2$ electrodes (alternatively, $xLi_2MnO_3\cdot(1-x)LiCrO_2$ [M′ = Mn; M = Cr; $x = 0.5$]) provided high capacity and good cycling stability at 50 °C when cells were charged and discharged between 4.4 and 2.5 V.[6,7] Our more recent efforts were influenced by reports that $LiMn_{0.5}Ni_{0.5}O_2$ and related lithium manganese−nickel oxides can provide capacities reaching 200 mA·h/g.[8−11] In particular, our approach is similar to that of Dahn et al.[10] who have studied the $Li[Ni_xLi_{(1/3-2x/3)}Mn_{(2/3-x/3)}]O_2$ system ($0 < x < 0.5$), which can be written, alternatively, in composite notation as $(1-2x)Li_2MnO_3\cdot(3x)LiMn_{0.5}$-

* To whom correspondence should be addressed. Email: thackeray@cmt.anl.gov.

(1) Rossouw, M. H.; Thackeray, M. M. *Mater. Res. Bull.* **1991**, *26*, 463.
(2) Rossouw, M. H.; Liles, D. C.; Thackeray, M. M. *J. Solid State Chem.* **1993**, *104*, 464.
(3) Tang, W.; Kanoh, H.; Yang, X.; Ooi, K. *Chem. Mater.* **2000**, *12*, 3271.
(4) Johnson, C. S.; Korte, S. D.; Vaughey, J. T.; Thackeray, M. M.; Bofinger, T. E.; Shao-Horn, Y.; Hackney, S. A. *J. Power Sources* **1999**, *81−82*, 491.
(5) Johnson, C. S.; Thackeray, M. M. *The Electrochem. Soc. Inc.*, PV 2000−36, **2001**, 47.
(6) Ammundsen, B.; Desilvestro, J.; Steiner, R.; Pickering, P. *10th International Meeting on Lithium Batteries*, Como, Italy, 28 May−2 June 2000; Ext. Abstr. No. 17.
(7) Ammundsen, B.; Paulsen, J. *Adv. Mater.* **2001**, *13*, 943.
(8) Spahr, M. E.; Novak, P.; Schnyder, B.; Haas, O.; Nesper, R. *J. Electrochem. Soc.* **1998**, *14*, 1113.
(9) Ohzuku, T.; Makimura, Y. *Chem. Lett.* **2001**, 744.
(10) Lu, Z.; MacNeil, D. D.; Dahn, J. R. *Electrochem. Solid State Lett.* **2001**, *4*, A191.
(11) Lu, Z.; Dahn, J. R. *J. Electrochem. Soc.* **2002**, *149*, A815.

10.1021/cm0306461 CCC: $27.50
Published on Web 04/20/2004

$Ni_{0.5}O_2$ (also for $0 < x < 0.5$). During the course of our studies, it was discovered that $LiMn_{0.5}Ni_{0.5}O_2$ and composite $xLi_2M'O_3\cdot(1-x)LiMn_{0.5}Ni_{0.5}O_2$ (M = Mn, Ti) electrode structures could accommodate an additional lithium within their structures at approximately 1.5 V vs Li^0 without disturbing the layered transition-metal framework structure.[12,13] This reaction, which is reversible, greatly increases the capacity of the layered electrode.

The structures of $xLi_2M'O_3\cdot(1-x)LiMO_2$ compounds (alternatively, in layered notation, $Li_{(2+2x)/(2+x)}M'_{2x/(2+x)}M_{(2-2x)/(2+x)}O_2$) appear to be complex. For example, magic angle spinning (MAS) nuclear magnetic resonance (NMR) and X-ray absorption spectroscopy (XAS) data of $Li_{1.2}Mn_{0.4}Cr_{0.4}O_2$ electrodes ($Li_2MnO_3\cdot LiCrO_2$) have provided evidence that the Li_2MnO_3 and $LiCrO_2$ components do not form a random solid solution, but rather that the structures tend to have short-range order with local clustering of the lithium and transition-metal ions.[14,15] Li_2MnO_3-like local environments or small domains were observed by NMR, which were electrochemically inert.[15] Similar Li_2MnO_3-like local environments were seen for $Li[Ni_xLi_{(1/3-2x/3)}Mn_{(2/3-x/3)}]O_2$ for $0 \le x \le 0.5$, but the Li ions in these environments participated in the electrochemistry, suggesting that the domains were smaller in size.[16] However, Dahn et al.[17] recently opposed the idea of Li_2MnO_3-like domains from analyses of XRD data and argued that the cations are arranged homogeneously within the layers of $Li[Cr_xLi_{(1-x)/3}Mn_{(2-2x)/3}]O_2$ for $0 \le x \le 1$ (alternatively, $(2-2x)Li_2MnO_3\cdot(3x)LiCrO_2$) and $Li[Ni_xLi_{(1/3-2x/3)}Mn_{(2/3-x/3)}]O_2$ for $0 \le x < 0.5$ (alternatively, $(1-2x)Li_2MnO_3\cdot(3x)LiMn_{0.5}Ni_{0.5}O_2$) structures, suggesting "a true solid solution phase."

In this paper, we address the ordering of these materials. For simplicity, we restrict the definition of structures in this paper, in most instances, to the composite notation $xLi_2M'O_3\cdot(1-x)LiMO_2$ rather than the equivalent layered notations used by Dahn et al.[10] We define and discuss $xLi_2M'O_3\cdot(1-x)LiMn_{0.5}Ni_{0.5}O_2$ electrode structures (M′ = Mn, Ti, or Zr; $0 \le x \le 0.3$) as determined by powder X-ray diffraction (XRD), high-resolution transmission electron microscopy (HRTEM), and MAS NMR. Electrochemical properties of the electrodes at both high potential (4.6−2.0 V) and at low potential (2.0−1.0 V) vs a metallic lithium reference electrode are presented. The electrochemical properties of electrodes containing a Li_2MnO_3 component are interpreted with reference to reports of the electrochemical activity that can be induced into Li_2MnO_3 by acid treatment[1,18] or by charging Li_2MnO_3 electrodes directly in lithium cells.[19]

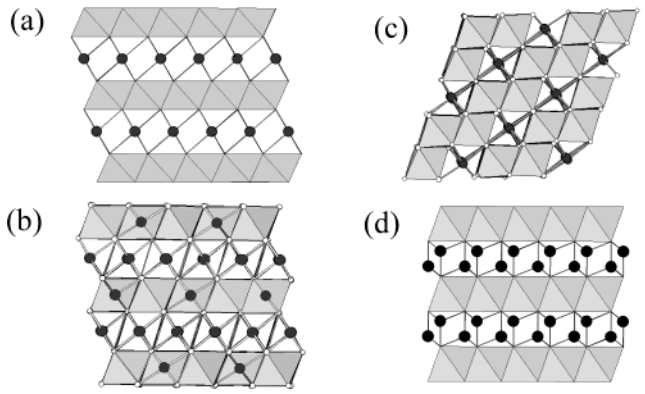

Figure 1. Schematic illustrations of the structures of (a) $LiMO_2$ (M = Mn, Ni, Co); (b) Li_2MnO_3 and Li_2TiO_3; (c) Li_2ZrO_3; (d) Li_2MO_2 (M = Mn, Ni).

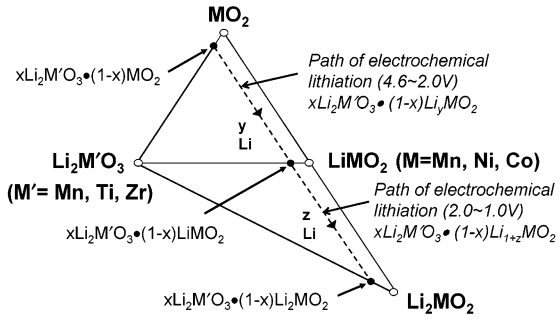

Figure 2. Compositional phase diagram of the Li_2MnO_3−MO_2−$LiMO_2$−Li_2MO_2 system.

To facilitate a discussion of the results, we first consider the structures of $xLi_2M'O_3\cdot(1-x)LiMO_2$ electrodes. Because of the structural similarities between $Li_2M'O_3$- and $LiMO_2$-type compounds, it was proposed several years ago that it might be possible to use an electrochemically inactive $Li_2M'O_3$ component, such as Li_2MnO_3, Li_2TiO_3, or Li_2ZrO_3, to stabilize $LiMO_2$ insertion electrodes (M = Co, Ni, Mn, and combinations thereof), particularly at low lithium loadings, by forming "composite" electrode structures, $xLi_2M'O_3\cdot(1-x)LiMO_2$.[2,4,20,21] In $LiCoO_2$, $LiNiO_2$, and $LiMnO_2$, the lithium and transition-metal ions are located in octahedral sites in alternating layers (Figure 1a), whereas in Li_2MnO_3 and Li_2TiO_3 (in layered notation, $Li[Li_{0.33}Mn_{0.67}]O_2$ and $Li[Li_{0.33}Ti_{0.67}]O_2$, respectively), one-third of the transition-metal ions are replaced by lithium (Figure 1b).[22] In Li_2ZrO_3, the structure is not layered because each cation layer contains Li^+ and Zr^{4+} ions in a 2:1 ratio (Figure 1c).[23]

The composition of $xLi_2M'O_3\cdot(1-x)LiMO_2$ electrodes for the complete range of x ($0 \le x \le 1$) is defined by the $Li_2M'O_3$−$LiMO_2$ tie-line in the schematic phase diagram of the $Li_2M'O_3$−MO_2−$LiMO_2$−Li_2MO_2 system in Figure 2. In ideal layered $Li_2M'O_3$ and $LiMO_2$ structures, such as Li_2MnO_3 and $LiCoO_2$, respectively, the cations in the transition-metal layers are perfectly ordered in layers between close-packed oxygen planes. Cation ordering

(12) Johnson, C. S.; Kim, J.-S.; Kropf, A. J.; Kahaian, A. J.; Vaughey, J. T.; Thackeray, M. M. *Electrochem. Commun.* **2002**, *4*, 492.
(13) Johnson, C. S.; Kim, J.-S.; Kropf, A. J.; Kahaian, A. J.; Vaughey, J. T.; Fransson, L. M.; Edstrom, K.; Thackeray, M. M. *Chem. Mater.* **2003**, *15*, 2313.
(14) Ammundsen, B.; Paulsen, J.; Davidson, I.; Liu, R.-S.; Shen, C.-H.; Chen, J.-M.; Jang, L.-Y.; Lee, J.-F. *J. Electrochem. Soc.* **2002**, *149*, A431.
(15) Pan, C. J.; Lee, Y. J.; Ammundsen, B.; Grey, C. P. *Chem. Mater.* **2002**, *14*, 2289.
(16) Yoon, W. S.; Paik, P.; Yang, X.-Q.; Balasubramanian, M.; McBreen, J.; Grey, C. P. *Electrochem. Solid State Lett.* **2002**, *5*, A263.
(17) Lu, Z.; Chen, Z.; Dahn, J. R. *Chem. Mater.* **2003**, *15*, 3214.
(18) Paik, Y.; Grey, C. P.; Johnson, C. S.; Kim, J.-S.; Thackeray, M. M. *Chem. Mater.* **2002**, *14*, 5109.
(19) Robertson, A. D.; Bruce, P. G. *Chem. Mater.* **2003**, *15*, 1984.
(20) Kim, J.-S.; Johnson, C. S.; Thackeray, M. M. *Electrochem. Commun.* **2002**, *4*, 205.
(21) Johnson, C. S.; Thackeray, M. M. In *Proc. 198th ECS Meeting*, Phoenix, AZ, 2000; Abstr. No. 67.
(22) Strobel, P.; Lambert, A. B. *J. Solid State Chem.* **1988**, *75*, 90.
(23) Hodeau, J. L.; Marezio, M.; Santoro, A.; Roth, R. S. *J. Solid State Chem.* **1982**, *45*, 170.

occurs in the Li_2Mn layers of Li_2MnO_3, which is driven by the large differences in charge of the monovalent and tetravalent Li and Mn ions, respectively. Therefore, when synthesizing compounds that fall on a $Li_2M'O_3$−$LiMO_2$ tie-line, it seems highly unlikely that perfectly ordered structures or superstructures with a homogeneous distribution of monovalent, divalent, trivalent, and/or tetravalent cations in the transition-metal layers will result, except at certain crystallographically allowed values of x. Furthermore, because it is extremely difficult to control the precise stoichiometry of lithiated metal oxide products at high synthesis temperatures, it is also highly likely that there will be variations in local composition in their structures, the extent of which will be dependent on (1) localized concentrations of lithium and transition-metal ions at the time of synthesis, (2) the oxygen content of the sample, and (3) the free energy of formation of various thermodynamically favored phases that will compete with one another at the synthesis temperature.

The $LiMn_{0.5}Ni_{0.5}O_2$ structure that has been used as the $LiMO_2$ component in the $xLi_2M'O_3\cdot(1-x)LiMn_{0.5}Ni_{0.5}O_2$ composite electrodes (M' = Mn, Ti, or Zr; $0 \le x \le 0.3$) of this investigation is of particular interest because the manganese and nickel ions adopt tetravalent and divalent oxidation states, respectively, rather than a trivalent state.[10] (Note that both Mn^{3+} (d^4) and Ni^{3+} (d^7) ions are Jahn−Teller active and that relaxation to undistorted states can therefore be achieved simultaneously by electron transfer from a Mn^{3+} ion to a neighboring Ni^{3+} ion.) Because manganese and nickel ions exist in the transition-metal layers of the $LiMn_{0.5}Ni_{0.5}O_2$ structure in a 1:1 ratio, there is no simple 3-fold (point group) symmetry in the transition-metal layers as there is in Li_2MnO_3. It is therefore impossible for every nickel ion to be surrounded by six manganese ions and vice versa. Therefore, if an ordered structure exists, there has to be another arrangement of the nickel and manganese ions.[24] Ceder et al.[25] have predicted by first-principles calculations that a zigzag arrangement of nickel and manganese has the lowest formation energy. However, no experimental crystallographic data has, to our knowledge, been provided that confirms the existence of the zigzag phase, presumably in part because materials synthesized to date contain Li ions in addition to Ni and Mn ions in the predominantly transition-metal layers. Yoon et al.[16,26] have demonstrated by MAS NMR that even in a $LiMn_{0.5}Ni_{0.5}O_2$ sample evidence could be found of local clustering and cation ordering in the transition-metal layers (i.e., Li_2MnO_3-type character), which was consistent with the presence of Ni ions in the lithium layers and vice versa, which is common in layered lithium−nickel oxides.[27] The spectra were rationalized by using a model based on Li_2MnO_3-like ordering, the Ni^{2+} substituting in sites that minimize the number of Li^+−Ni^{2+} contents in the transition-metal layers.[28] Some evidence for Ni^{2+} clustering, presumably in $LiNi_{0.5}Mn_{0.5}O_2$ regions, was also observed for $0.3 \le x < 0.5$.[28]

Ohzuku has predicted by first-principles calculations that a $\sqrt{3} \times \sqrt{3}$ supercell should exist in a $LiMn_{0.33}Ni_{0.33}Co_{0.33}O_2$ structure.[29] Dahn et al.[17] claim from analyses of powder X-ray diffraction data that a similar $\sqrt{3} \times \sqrt{3}$ supercell exists for $Li[Ni_xLi_{(1/3-2x/3)}Mn_{(2/3-x/3)}]O_2$ samples ($0 < x \le 0.5$) (alternatively, $(1-2x)Li_2MnO_3\cdot(3x)LiMn_{0.5}Ni_{0.5}O_2$) but assert that because the lattice parameters change continuously with x, the cations are homogeneously distributed in the transition-metal layers over a wide range of x.

During our initial studies of $LiMn_{0.5}Ni_{0.5}O_2$ and $0.03Li_2TiO_3\cdot0.97LiMn_{0.5}Ni_{0.5}O_2$ electrodes, it was discovered that an additional lithium ion could be inserted into the $LiMn_{0.5}Ni_{0.5}O_2$ component below 2 V vs Li^0 to yield a $Li_2Mn_{0.5}Ni_{0.5}O_2$ structure without destroying the layered arrangement of the electrode structure (Figure 1d).[12,13] In $Li_2Mn_{0.5}Ni_{0.5}O_2$, which is isostructural with Li_2MnO_2[30] and Li_2NiO_2,[31] the manganese and nickel ions maintain their octahedral configuration, whereas the lithium ions fully occupy the tetrahedral sites in adjacent layers. The Li_2MO_2 composition is included in the compositional phase diagram in Figure 2 because, in principle, such structures can significantly increase the capacity of composite $xLi_2M'O_3\cdot(1-x)LiMO_2$ electrodes at potentials below 2 V vs Li^0.

Experimental Section

Synthesis of $xLi_2M'O_3\cdot(1-x)LiMn_{0.5}Ni_{0.5}O_2$ Electrodes. Electrode materials defined by the general composition $xLi_2M'O_3\cdot(1-x)LiMn_{0.5}Ni_{0.5}O_2$ (M' = Ti, Mn, and Zr) were prepared for $x = 0.03$, 0.07, 0.14, and 0.30. Electrodes in which M' = Ti or Zr were prepared by reacting the appropriate amounts of anatase (TiO_2, Aldrich), titanium isopropoxide ($Ti[OCH(CH_3)_2]_4$, Aldrich), or zirconium isopropoxide 2-propanol complex ($Zr[OCH(CH_3)_2]_4\cdot(CH_3)_2CHOH$, Aldrich) with lithium hydroxide monohydrate ($LiOH\cdot H_2O$, Aldrich) and $Ni_{0.5}Mn_{0.5}(OH)_2$. Electrodes in which M' = Mn were prepared directly from $Ni_{1-x}Mn_x(OH)_2$ and $LiOH\cdot H_2O$ using the required Li:Mn:Ni ratio. The $Ni_{0.5}Mn_{0.5}(OH)_2$ and $Ni_{1-x}Mn_x(OH)_2$ precursors were prepared in-house by precipitation from a basic LiOH solution of $Ni(NO_3)_2$ and $Mn(NO_3)_2$ (pH ∼ 11). The reagents were intimately mixed in an acetone slurry, dried in an oven overnight, and subsequently fired at 480 °C for 12 h and then at 900 °C for 10 h in air. Thereafter, the samples were rapidly quenched (also in air). Powder X-ray diffraction patterns of the products were collected on a Siemens D5000 powder diffractometer with Cu Kα radiation between 10° and 80° 2θ at a scan rate of 0.6° 2θ/min. Lattice parameters of the phases were determined by Rietveld profile refinements of the X-ray diffraction patterns.

High-Resolution Transmission Electron Microscopy. High-resolution images of $xLi_2TiO_3\cdot(1-x)LiMn_{0.5}Ni_{0.5}O_2$ and $xLi_2MnO_3\cdot(1-x)LiMn_{0.5}Ni_{0.5}O_2$ structures were obtained for $x = 0$, 0.14, and 0.30. Samples were prepared for the electron microscope by a standard procedure described elsewhere.[32] The images were collected on a JEOL-JEM 4000FEX-1 transmis-

(24) Islam, M. S.; Davies, R. A.; Gale, J. D. *Chem. Mater.* **2003**, *15*, 4280.
(25) Ceder, G.; Carlier, D.; Grey, C. P.; Gorman, J. P.; Reed, J. *Lithium Battery Discussion Workshop*, Arcachon, France, 14−19 September 2003; Ext. Abstr. No. 53.
(26) Yoon, W.-S.; Grey, C. P.; Balsubramanian, M.; Yang, X.-Q.; McBreen, J. *Chem. Mater.* **2003**, *15*, 3161.
(27) Delmas, C. In *Lithium Batteries, New Materials, Developments, and Perspectives*; Pistoia, G., Ed.; Elsevier: Amsterdam, 1994; p 457.
(28) Yoon, W.-S.; Iannopollo, S.; Grey, C. P.; Carlier, D.; Gorman, J.; Reed, J.; Ceder, G. *Electrochem. Solid State Lett.*, in press.
(29) Koyama, Y.; Tanaka, I.; Adachi, H.; Makimura, Y.; Ohzuku, T. *J. Power Sources* **2003**, *119*−*121*, 644.
(30) David, W. I. F.; Goodenough, J. B.; Thackeray M. M.; Thomas, M. G. S. R. *Rev. Chem. Miner.* **1983**, *20*, 636.
(31) Dahn, J. R.; von Sacken, U.; Michal, C. A. *Solid State Ionics* **1990**, *44*, 87.
(32) Shao-Horn, Y.; Hackney, S. A.; Cornilsen, B. C. *J. Electrochem. Soc.* **1997**, *144*, 3147.

sion electron microscope under an accelerating voltage of 200 keV. The images were produced without an objective aperture to produce phase contrast. Fourier transform analysis was carried out using Scion Image (Scion Corp., Release Beta 4.0.2) on a 64 × 64 pixel section of the digital image file.

Magic Angle Spinning Nuclear Magnetic Resonance. ^{6}Li MAS NMR data of $xLi_2TiO_3\cdot(1-x)LiMn_{0.5}Ni_{0.5}O_2$ samples ($x = 0$, 0.14, and 0.30) were collected at 29.5 MHz on a CMX-200 spectrometer, with a spinning speed of 38 kHz and rotor synchronized spin−echoes ($\pi/2 - \tau - \pi - \tau -$ acq.; τ = one rotor period; $\pi/2 = 2\ \mu$s). The spectra were referenced to 1 M LiCl at 0 ppm.

Electrochemical Measurements. Electrodes were fabricated by intimately mixing 85 wt % of the appropriate $xLi_2M'O_3\cdot(1-x)LiMn_{0.5}Ni_{0.5}O_2$ powder, 8 wt % poly(vinylidene difluoride) (PVDF) binder (Kynar, Elf-Atochem), and 7 wt % acetylene black (Cabot) in a 1-methyl-2-pyrrolidinone (NMP) solvent (Aldrich, 99+%). The mixed slurry was cast onto an aluminum foil current collector and dried at 75 °C for 3−5 h. The electrode laminates were dried further at 70 °C under vacuum overnight. Disk electrodes with an area of 1.6 cm^2 were punched from the laminates. The electrodes were evaluated in coin-type cells (size 2032, Hohsen Corp.) with lithium foil (FMC Corp.) as the counter electrode, a polypropylene separator (Celgard), and an electrolyte solution consisting of 1 M $LiPF_6$ in a 1:1 ethylene carbonate:diethyl carbonate solvent mixture (Merck). Cells were constructed inside a helium-filled glovebox (<5 ppm, H_2O and O_2). Cells were cycled galvanostatically using a Maccor Series 2000 control unit at a current rate of 0.1 mA/cm^2.

Results

XRD Patterns. The powder XRD patterns of $xLi_2M'O_3\cdot(1-x)LiMn_{0.5}Ni_{0.5}O_2$ electrodes for M′ = Mn, Ti, or Zr and $0 \le x \le 0.3$ are provided in Figure 3. Because of the paucity of data, lattice parameters were refined using the high-symmetry trigonal space group, $R\bar{3}m$, rather than the low-symmetry monoclinic space group, $C2/m$, to monitor the variations in unit cell dimensions as a function of composition, x (Table 1). The XRD patterns of the $xLi_2MnO_3\cdot(1-x)LiMn_{0.5}Ni_{0.5}O_2$ ($x = 0.00$, 0.03, 0.14, and 0.30) composite structures in Figure 3a are similar. Figure 3a shows a slight increase in intensity of the peaks at 20−23° 2θ as the Li_2MnO_3 component in the structure increases, which is consistent with an increasing amount of lithium in the transition-metal layers. Our XRD patterns and the changes in lattice parameter are consistent with those reported by Dahn et al.[17] for $Li[Ni_xLi_{(1/3-2x/3)}Mn_{(2/3-x/3)}]O_2$ electrodes; the smooth variation in lattice parameter with composition was interpreted by this group as suggesting that these materials are structurally and chemically homogeneous. Overall, the average unit cell parameters and unit cell volumes decrease marginally with increasing Mn content, which is consistent with the difference in the ionic radii between Mn^{4+} (0.54 Å) and Ni^{2+} (0.69 Å) ions in octahedral coordination.[33] By contrast, the average lattice parameters and unit cell volumes of $xLi_2TiO_3\cdot(1-x)LiMn_{0.5}Ni_{0.5}O_2$ products synthesized from a $Ti[OCH(CH_3)_2]_4$ precursor increase in value with increasing x; in this case, the trend is consistent with the larger ionic radius of Ti^{4+} (0.61 Å) compared to Mn^{4+} (0.54 Å). The patterns in Figure 3a,b emphasize the structural compatibility that exists among Li_2MnO_3, Li_2TiO_3, and $LiMn_{0.5}Ni_{0.5}O_2$ phases and the ability of the $Li_2M'O_3$-type component to become integrated into a $LiMO_2$-type structure. However, when TiO_2 (anatase) was used as a precursor, the XRD patterns of the $xLi_2TiO_3\cdot(1-x)LiMn_{0.5}Ni_{0.5}O_2$ products showed two-phase character, which is clearly noticeable, for $x = 0.3$, at approximately 44° 2θ in Figure 3c, suggesting that the Li_2TiO_3 component is not integrated to the same extent into the $LiMn_{0.5}Ni_{0.5}O_2$ structure as it is in the products in Figure 3b. This observation clearly emphasizes that the structural integration of $Li_2M'O_3$ and $LiMn_{0.5}Ni_{0.5}O_2$ components depends strongly on the type of reagents used and on the reaction conditions during synthesis.

Table 1. Lattice Parameters of $xLi_2M'O_3\cdot(1-x)LiMn_{0.5}Ni_{0.5}O_2$ Structures (M′ = Mn, Ti, Zr)

x	a (Å)	c (Å)	vol (Å^3)
	$xLi_2MnO_3\cdot(1-x)LiMn_{0.5}Ni_{0.5}O_2$		
0.03	2.870(1)	14.259(3)	101.69(2)
0.14	2.864(1)	14.246(2)	101.21(2)
0.30	2.859(1)	14.246(2)	100.85(2)
	$xLi_2TiO_3\cdot(1-x)LiMn_{0.5}Ni_{0.5}O_2$		
0.03	2.876(1)	14.274(2)	102.22(1)
0.14	2.881(1)	14.304(2)	102.78(2)
0.30	2.887(1)	14.342(2)	103.52(2)
	$xLi_2ZrO_3\cdot(1-x)LiMn_{0.5}Ni_{0.5}O_2$		
0.03	2.873(1)	14.259(2)	101.94(2)

The X-ray diffraction patterns of $xLi_2ZrO_3\cdot(1-x)LiMn_{0.5}Ni_{0.5}O_2$ products showed that the $LiMn_{0.5}Ni_{0.5}O_2$ structure is less tolerant to accommodating Li_2ZrO_3. Although the $0.03Li_2ZrO_3\cdot0.97LiMn_{0.5}Ni_{0.5}O_2$ electrode had an X-ray diffraction pattern similar to those of its M′ = Mn and Ti analogues (Figure 3d), $xLi_2ZrO_3\cdot(1-x)LiMn_{0.5}Ni_{0.5}O_2$ products with higher Li_2ZrO_3 content ($x > 0.03$) were multiphase, as were those of $xLi_2MnO_3\cdot(1-x)LiMn_{0.5}Ni_{0.5}O_2$ and $xLi_2TiO_3\cdot(1-x)LiMn_{0.5}Ni_{0.5}O_2$ products for $x > 0.3$ (not shown). We are unsure of the structural features of $0.03Li_2ZrO_3\cdot0.97LiMn_{0.5}Ni_{0.5}O_2$, and we do not know yet if, at this low concentration, the Li_2ZrO_3 component is embedded within the bulk of the $LiMn_{0.5}Ni_{0.5}O_2$ structure or whether it exists as an independent phase. We attribute the difficulty in integrating Li_2ZrO_3 into a layered $LiMn_{0.5}Ni_{0.5}O_2$ structure to (1) the absence of lithium layering in Li_2ZrO_3 (Figure 1c) and (2) the relatively large second-row transition-metal ion, Zr^{4+} (ionic radius = 0.72 Å).[33]

Although refinements of the XRD patterns showed that the lattice parameters of both $xLi_2MnO_3\cdot(1-x)LiMn_{0.5}Ni_{0.5}O_2$ and $xLi_2TiO_3\cdot(1-x)LiMn_{0.5}Ni_{0.5}O_2$ systems changed gradually with x, which is consistent with increasing amounts of Li_2MnO_3 and Li_2TiO_3, respectively, X-ray diffraction is not a sufficiently sensitive technique for determining the local variations in composition and structure in these materials. We therefore relied on more sensitive techniques, such as HRTEM and NMR, to obtain a more detailed understanding of the local structure of these materials at a nanoscopic level.

HRTEM Analyses. The HRTEM images of structures in the $xLi_2MnO_3\cdot(1-x)LiMn_{0.5}Ni_{0.5}O_2$ and $xLi_2TiO_3\cdot(1-x)LiMn_{0.5}Ni_{0.5}O_2$ systems were examined at three compositions, $x = 0.0$, 0.14, and 0.30. To accommodate the diffraction peaks that occur between 20° and 23° 2θ in the XRD patterns of these compounds, the indexing of the lattice fringes was based on the mono-

(33) Shannon, R. D.; Prewitt, C. T. *Acta Crystallogr.* **1969**, *B25*, 925.

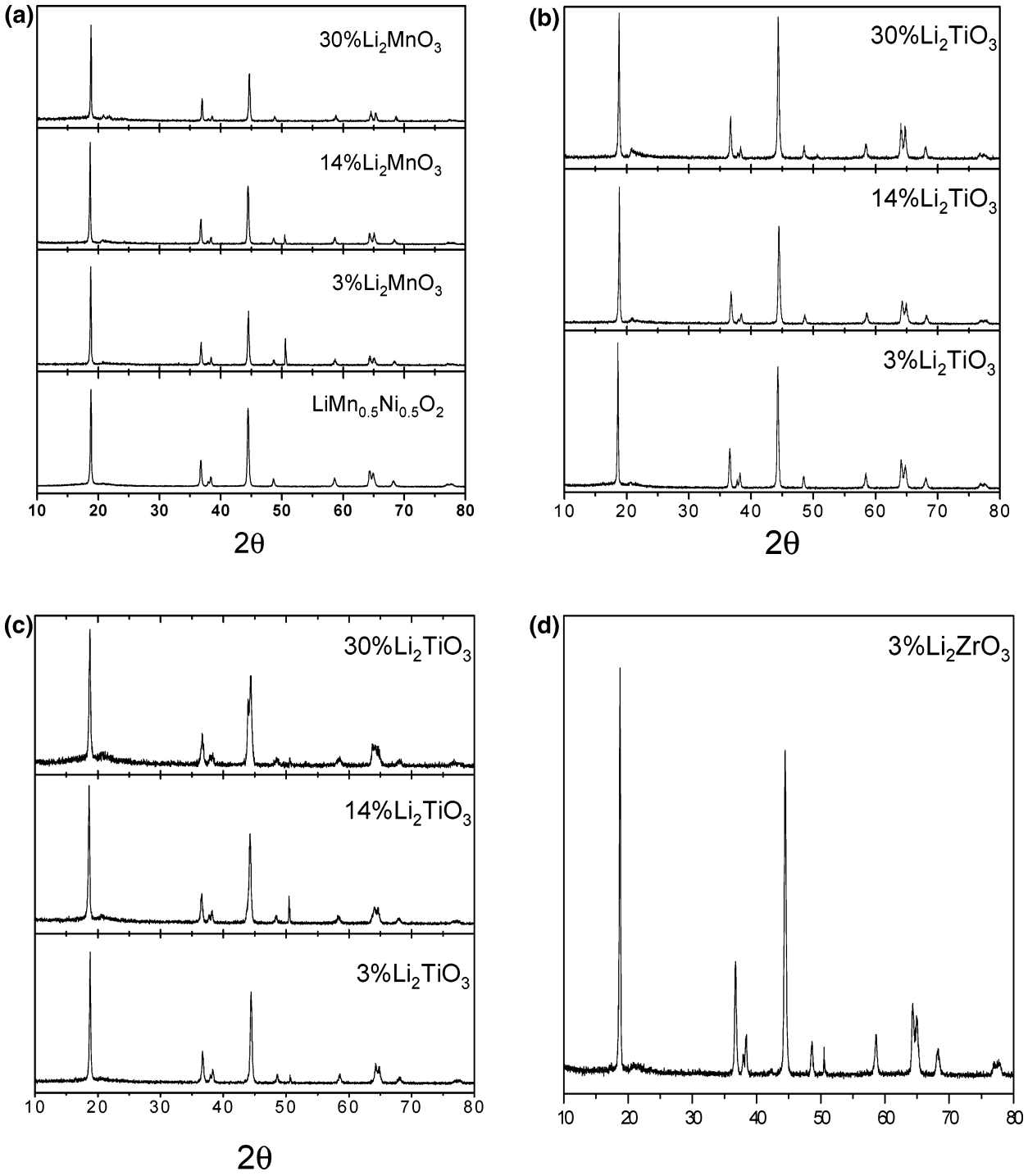

Figure 3. Powder X-ray diffraction patterns of $x\mathrm{Li_2M'O_3}\cdot(1-x)\mathrm{LiMn_{0.5}Ni_{0.5}O_2}$ structures: (a) $x\mathrm{Li_2MnO_3}\cdot(1-x)\mathrm{LiMn_{0.5}Ni_{0.5}O_2}$ (x = 0.0, 0.03, 0.14, 0.30); (b) $x\mathrm{Li_2TiO_3}\cdot(1-x)\mathrm{LiMn_{0.5}Ni_{0.5}O_2}$ (x = 0.03, 0.14, 0.30) ($\mathrm{Ti[OCH(CH_3)_2]_4}$ precursor); (c) $x\mathrm{Li_2TiO_3}\cdot(1-x)\mathrm{LiMn_{0.5}Ni_{0.5}O_2}$ (x = 0.03, 0.14, 0.30) ($\mathrm{TiO_2}$ precursor); (d) $x\mathrm{Li_2ZrO_3}\cdot(1-x)\mathrm{LiMn_{0.5}Ni_{0.5}O_2}$ (x = 0.03).

clinic unit cell ($C2/m$) defined by Strobel et al.[22] for $\mathrm{Li_2MnO_3}$.

The examination of the X-ray diffraction patterns of these materials shows the same type of "superlattice" peaks between 20° and 23° 2θ as described by Dahn et al.[17] for the $\mathrm{Li[Ni_xLi_{(1/3-2x/3)}Mn_{(2/3-x/3)}]O_2}$ system ($0 < x < 0.5$). These peaks are of particular importance to the local (nearest cation neighbor) environment of the Li ions because the peak intensities are a rationalization of the ordering of the lithium, manganese, and other transition-metal ions present in the transition-metal layers. However, an ideal superlattice can occur only if the atomic distribution is uniform on a length scale approaching that of the superlattice length and if the ions occur in exactly the correct proportion. When such an ideal superlattice occurs, it is expected that the broadening of the superlattice peaks will correspond to the same crystallite size as that determined from "nonsuperlattice" peaks. If, however, the composition is nonideal in the sense that it deviates from that required by an ideal superlattice, or if the composition is not spatially uniform, then the superlattice peaks will be weakened and broadened.[34] This is of specific concern to this work because of the observations of relatively

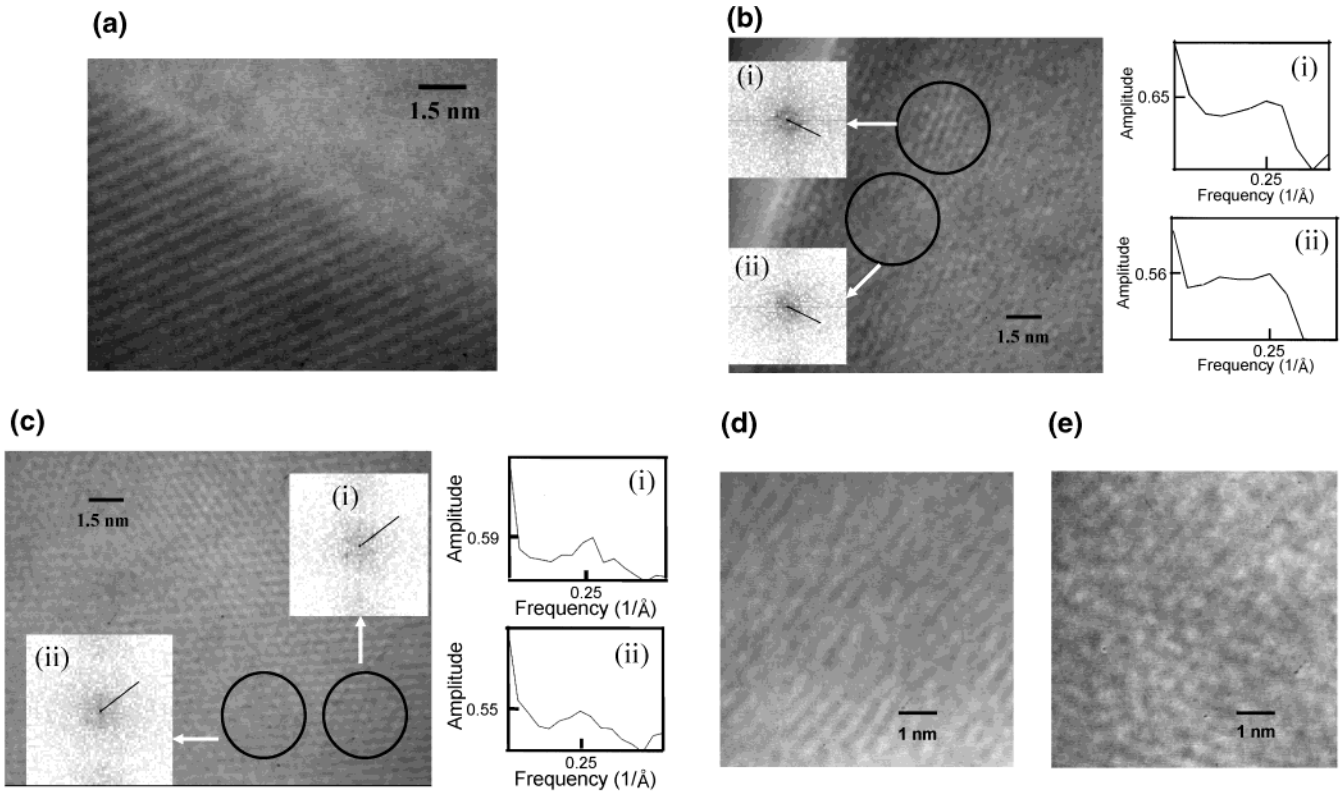

Figure 4. (a) $LiMn_{0.5}Ni_{0.5}O_2$ lattice fringes associated with (001) peak ($C2/m$). (b) HRTEM image of $LiMn_{0.5}Ni_{0.5}O_2$ formed using phase contrast from superlattice peaks and local fast Fourier transforms (inset) from adjacent areas (i) and (ii) to emphasize the spatial variation in superlattice order parameter. (c) HRTEM image of $0.30Li_2MnO_3 \cdot 0.70LiMn0.5Ni_{0.5}O_2$ formed using phase contrast from superlattice peaks and fast Fourier transforms (inset) from adjacent areas (i) and (ii) to emphasize the spatial variation in superlattice order parameter. (d) Lattice fringe images in $0.14Li_2TiO_3 \cdot 0.86LiMn_{0.5}Ni_{0.5}O_2$. (e) Lattice fringe images in $0.30Li_2TiO_3 \cdot 0.70LiMn_{0.5}Ni_{0.5}O_2$.

broad superlattice lines in the nonideal compound compositions, for example, $xLi_2M'O_3 \cdot (1-x)LiMO_2$ compositions $x = 0.14$ and $x = 0.30$. In such cases, where relatively broad superlattice peaks are observed, two different structural models can be used to rationalize the observation. We may consider either (1) that the broadening is due to isolated regions of composition close to what is ideal for superlattice formation surrounded by disordered regions of nonideal composition[35] or (2) that the composition is uniform, but that the ordered structure is interrupted by anti-phase domain boundaries.[36] In either case, there will be variations in the local environment of Li compared to the ideal superlattice. We therefore resorted to HRTEM to provide further evidence for the existence of such nonuniformities in the superlattice, as suggested by the broadening of the superlattice peaks in Figure 3a,b. Using this technique, it is possible to directly image the superlattice structure corresponding to the peaks at 20−23° 2θ.

Figure 4a shows the lattice fringes of a $LiMn_{0.5}Ni_{0.5}O_2$ structure associated with the close-packed 001 planes of the monoclinic unit cell ($d \approx 4.7$ Å), which are equivalent to the 003 planes of the trigonal ($R\bar{3}m$) unit cell of $LiCoO_2$. The image shows well-behaved packing of these planes, as might be expected in a stoichiometric $LiMn_{0.5}Ni_{0.5}O_2$ structure. However, if the crystals are at orientations that allow the possibility of coherent diffraction from the superlattice structure, then fringes of weak contrast and discontinuous morphology corresponding to the "superlattice" peaks at 20−23 °2θ (i.e., the (020) and (110) peaks, $d \approx 4.3$ Å) are observed within a single grain of $LiMn_{0.5}Ni_{0.5}O_2$ (Figure 4b). The nanoscale, spatial variation in the lattice fringe contrast suggests that, even in the parent $LiMn_{0.5}Ni_{0.5}O_2$ structure, the distribution of the cations in the transition-metal layers is not random or homogeneous. We also note that the existence of the discontinuous superlattice structure for $LiMn_{0.5}Ni_{0.5}O_2$ observed here by HRTEM is indeed consistent with the MAS NMR results,[16,26] but would be difficult to predict using isolated X-ray diffraction spectra.

In an attempt to have a more quantitative measure of the structure and chemistry variations suggested in Figure 4b, two adjacent areas are circled in Figure 4b for specific consideration. Qualitatively, it is observed that the lattice fringes corresponding to the superlattice structure show greater definition in region (i) compared to region (ii). This observation is relevant because the amplitude of contrast of the lattice fringes is proportional to the superlattice structure factor.[37] Assuming that the crystallographic orientation and crystal thickness are approximately the same for these adjacent regions, the variation in lattice fringe contrast implies a spatial variation in the structure factor for the superlattice. A more quantitative demonstration of the

(34) Guinier, A. *X-ray Diffraction*; W. H. Freeman and Company: San Francisco, CA, 1963; p 254.
(35) Rhines, F. M.; Newkirk, J. B. *Trans. ASM* **1953**, *45*, 1029.
(36) Jones, F. W.; Sykes, G. *Proc. R. Soc. London A* **1938**, *166*, 376.
(37) Williams, D. B.; Carter, C. B. *Transmission Electron Microscopy*; Plenum Press: New York, 1996; p 441.

contrast in the lattice fringes in regions (i) and (ii) is provided by two-dimensional Fourier transforms applied locally to the circled regions in Figure 4b. The gray scale of the pixels in the Fourier transform plot measures the amplitude of the corresponding frequencies with the origin normalized to maximum density. If the gray scale is plotted along a line drawn from the origin (center) of the two-dimensional Fourier transform, perpendicular to the lattice fringes, a quantitative measure of the amplitude of the fringe contrast is obtained as a function of spatial frequency, as shown on the right of Figure 4b. The spatial frequency corresponding to the superlattice periodicity is indicated on the line profiles. A quantitative measure of the ratio of the structure factor of region (i) to region (ii) is 1.15 ± 0.01, suggesting a change in composition and/or short-range order between the two regions. The presence of nanoscale domains defined by local variations in a superlattice order parameter are consistent with the very weak, broad, and ill-defined superlattice peaks that occur between 20° and 23° 2θ in the X-ray diffraction patterns of xLi$_2$M′O$_3$·(1−x)LiMn$_{0.5}$Ni$_{0.5}$O$_2$ samples.

Figure 4c shows the structural image of a 0.30Li$_2$MnO$_3$·0.70LiMn$_{0.5}$Ni$_{0.5}$O$_2$ sample formed from overlapping lattice fringes from the diffraction peaks at 20−23° 2θ, which were significantly stronger than the peaks of the parent LiMn$_{0.5}$Ni$_{0.5}$O$_2$ sample (Figure 3a). Thus, it is not surprising that the continuity and contrast amplitude of the lattice-fringe image is qualitatively superior to that observed in LiMn$_{0.5}$Ni$_{0.5}$O$_2$. However, it is still apparent that a nanoscale spatial variation in amplitude contrast is also present in Figure 4c. In a manner analogous to the examination performed in Figure 4b, the local Fourier transform of the indicated regions in Figure 4c was used to quantify the spatial variation in amplitude. In this case, the ratio of the structure factor of region (i) to region (ii) was determined to be 1.09 ± 0.01. The HRTEM data presented in Figures 4b,c provide evidence that these materials are not structurally homogeneous at the nanometer scale. Instead, the interpretation of the images of the superlattice suggests a spatially varying structure factor that is more consistent with a nanometer-scale domain structure. We argue that such observations are entirely consistent with the occurrence of the weak and broad superlattice reflections in the X-ray diffraction patterns.

The atomic heterogeneity in the transition-metal layers is exacerbated in the images of xLi$_2$TiO$_3$·(1−x)-LiMn$_{0.5}$Ni$_{0.5}$O$_2$ structures in Figure 4d (x = 0.14) and Figure 4e (x = 0.30), which show strong perturbations in the lattice fringes. These images are more consistent with a structural model with short-range order and domain-type features rather than the "true solid solution" proposed by Dahn et al.[17] Interestingly, the 0.30Li$_2$MnO$_3$·0.7LiMn$_{0.5}$Ni$_{0.5}$O$_2$ structure (Figure 4c) appears to be better behaved than its Ti counterpart (Figure 4e).

MAS NMR Data. ^{6}Li MAS NMR data of xLi$_2$TiO$_3$·(1-x)LiMn$_{0.5}$Ni$_{0.5}$O$_2$ samples were collected for x = 0.03, 0.07, 0.14, and 0.30 (Figure 5a−e). The x = 0.03 spectrum (Figure 5a) is similar to that of x = 0.[16] Three groups of resonances are clearly observed: one at 1600−1300 ppm, the second and more intense group at approximately 800−500 ppm, and the third at 0 ppm.

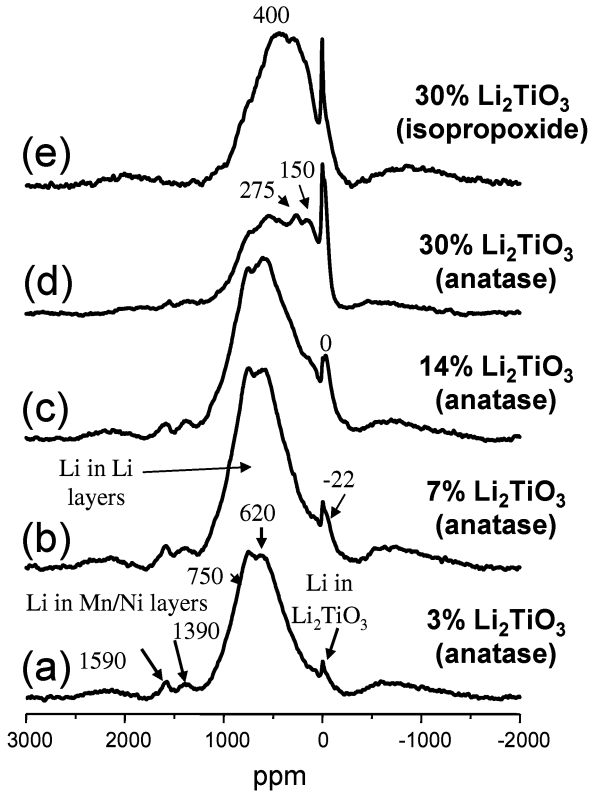

Figure 5. ^{6}Li MAS NMR spectra of xLi$_2$TiO$_3$·(1−x)LiMn$_{0.5}$-Ni$_{0.5}$O$_2$ for x = 0.03, 0.07, 0.14, and 0.3 prepared with anatase as the titanium source (a−d). The x = 0.3 sample synthesized with titanium isopropoxide as the titanium source is shown for comparison (e). Spectra were acquired with spinning speeds of 38 kHz.

The first group is assigned to Li local environments in the transition-metal layers: the resonance at ∼1590 ppm is due to the environment Li(OMn)$_6$ (where only the cations in the first cation coordination shell in the transition-metal layers are considered), which is present in Li$_2$MnO$_3$, and the broader resonance at ∼1390 ppm to Li(OMn$_5$Ni). These two resonances are a clear signature for local Li$^+$:Mn^{4+}, "Li$_2$MnO$_3$-like" cation ordering. The intermediate frequency, broader resonances are assigned to Li in the Li layers. The resonance at ∼0 ppm is attributed to Li in a diamagnetic local environment, as found, for example, in Li$_2$TiO$_3$. The shoulder to lower frequency of the 0 ppm resonance (centered at −22 ppm) is attributed to environments with Ni^{2+} ions in the first coordination sphere, based on an earlier NMR study of LiNi$_{0.5}$Ti$_{0.5}$O$_2$.[38] For example, the local environments in the transition-metal layers Li(OM^{4+})$_5$(ONi^{2+}) will give rise to a resonance at ∼1390 ppm when M = Mn and at −21 to −30 ppm when M = Ti. As the Ti content increases, for the samples prepared with anatase, the resonance centered at ∼620 ppm grows in intensity and new, broad resonances at lower frequencies emerge at ∼150 and ∼275 ppm. The latter two resonances are more clearly seen for the x = 0.3 sample. Again based on earlier work, these are assigned to Li environments in the Li layers that contain one (150 ppm) and two (275 ppm) Ni^{2+} ions in the second cation coordination environment and no Mn^{4+} ions.[38] These environments will

(38) Carlier, D.; Kang, K.; Ceder, G.; Yoon, W. S.; Grey, C. P. In *ECS Proceedings*, Paris, 2003.

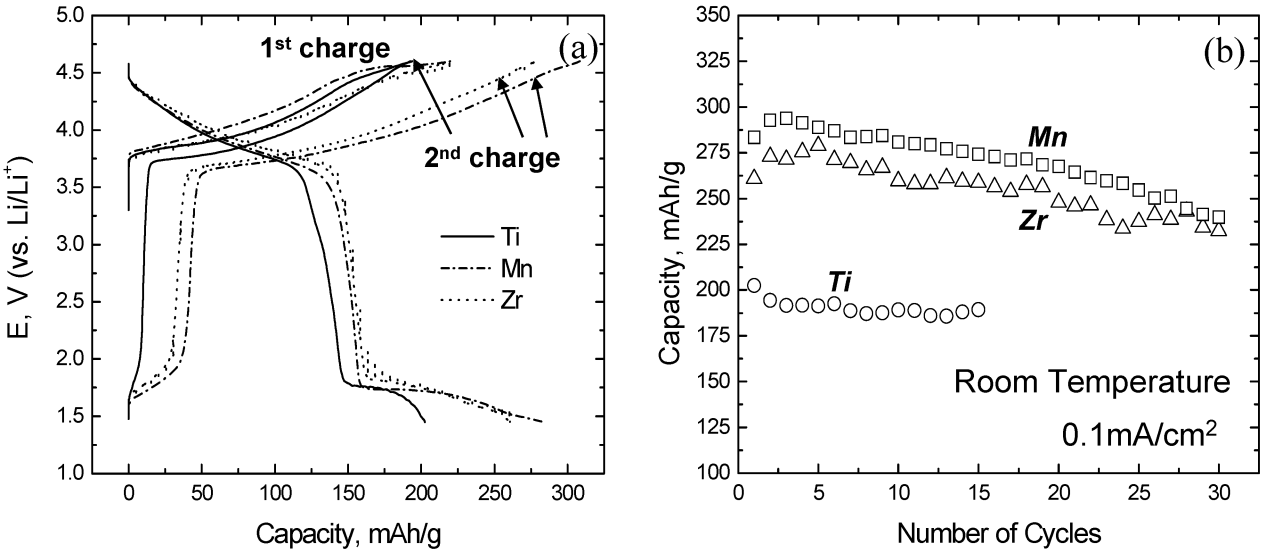

Figure 6. Voltage profiles (a) and capacity vs cycle number plots (b) of $Li/0.03Li_2M'O_3\cdot0.97LiMn_{0.5}Ni_{0.5}O_2$ cells ($M' = Mn, Ti, Zr$) between 4.60 and 1.45 V at room temperature.

exist if Li_2TiO_3 particles or domains exist in the sample that are substituted by Ni^{2+}. The resonance at 275 ppm may also contain a contribution from the local environment that results from Mn^{4+} substitution of the Li_2TiO_3 domains and which contains only one Mn^{4+} ion in the first cation coordination sphere (and only Li/Ti in the second coordination shell). The resonance at ~620 ppm is assigned to the Li_2MnO_3-like environment where one Mn^{4+} ion in the first coordination shell has been substituted by Ti^{4+} or Ni^{2+}. The growth of this resonance with Ti content is, therefore, ascribed to Ti^{4+} substitution. The high-frequency resonances at 1590−1390 ppm decrease as a function of Ti content, indicating that an increasing number of Li environments in the transition-metal layers $Li(Mn_{6-x-y}Ni_xTi_y)$ must contain Ti^{4+}. This is consistent with the incorporation of some Li_2TiO_3 into the $LiNi_{0.5}Mn_{0.5}O_2$ structure.

The spectra of the $x = 0.3$ samples in Figure 5d,e can be clearly interpreted in terms of structures containing segregated "$LiMn_{0.5}Ni_{0.5}O_2$-doped Li_2TiO_3" domains/crystallites or "Li_2TiO_3-doped $LiMn_{0.5}Ni_{0.5}O_2$" domains/crystallites. The degree of mixing between the Li_2TiO_3 and $LiMn_{0.5}Ni_{0.5}O_2$ components increases dramatically for the $x = 0.3$ sample prepared with Ti isopropoxide (Figure 5e) in comparison to the sample made from TiO_2 (anatase, Figure 5d). The resonances due to $LiMn_{0.5}Ni_{0.5}O_2$- and Li_2TiO_3-rich regions decrease and instead a broad resonance centered at about 400 ppm is observed. Furthermore, the high-frequency resonances have disappeared, indicating that any Li^+:M^{4+} ordering must now involve both Ti^{4+} and Mn^{4+}. However, a sharp resonance with a downfield shoulder is still observed at 0 ppm, indicating that some discrete Li_2TiO_3-like domains/crystallites still remain.

Electrochemistry. The change in composition of $xLi_2M'O_3\cdot(1-x)LiMO_2$ electrodes that occurs during an electrochemical reaction with lithium is shown in the schematic phase diagram in Figure 2. The composition of layered $LiMO_2$ electrodes (M = Co, Ni, Mn) changes, on lithium extraction, along the $LiMO_2-MO_2$ tie-line. For $LiCoO_2$ and $LiNiO_2$, lithium extraction is limited by high oxygen activity at the electrode surface that destabilizes their structures when approximately one-half of the lithium ions have been removed. On the other hand, delithiation of $LiMnO_2$ is accompanied by a migration of manganese into the lithium-depleted layers to form a spinel-type structure, which compromises the high-potential behavior of the electrode.[39] By integrating electrochemically inactive $Li_2M'O_3$ components, such as Li_2TiO_3 and Li_2ZrO_3, with strong Ti−O and Zr−O bonds into the $LiMO_2$ electrode, it was hoped that composite $xLi_2M'O_3\cdot(1-x)LiMO_2$ structures would provide greater stability to lithium insertion/extraction reactions and, in particular, that $xLi_2M'O_3\cdot(1-x)LiMnO_2$ electrodes would help suppress the transformation of the layered $LiMnO_2$ component to spinel. For $xLi_2M'O_3\cdot(1-x)LiMO_2$ electrodes, the composition changes on lithium extraction along the dashed $xLi_2M'O_3\cdot(1-x)LiMO_2-xLi_2M'O_3\cdot(1-x)MO_2$ tie-line in Figure 2. If the $Li_2M'O_3$ component is electrochemically inactive, it stands to reason that the concentration of $Li_2M'O_3$ used should be as small as possible to maximize the capacity of the electrode. Lithium insertion into the $LiMO_2$ component drives the composition of the electrode toward $xLi_2M'O_3\cdot(1-x)Li_2MO_2$, with the Li_2MO_2 component controlling the low-voltage behavior of the $xLi_2M'O_3\cdot(1-x)LiMO_2$ electrode.

The electrochemical profiles and plots of cycling stability of $Li/xLi_2M'O_3\cdot(1-x)LiMn_{0.5}Ni_{0.5}O_2$ cells (M = Mn, Ti, Zr) for $x = 0.03$ and $x = 0.30$, when cycled between 4.6 and 1.45 V vs Li^0, are shown in Figures 6−8. Figure 6a shows the first two charge profiles and the initial discharge profile of the cells at room temperature; the cycling stability of the composite electrodes for the first 30 cycles is shown in Figure 6b. The data are similar for the electrodes in which $M' = Mn$ and Zr. The similarity in electrochemical behavior is consistent with the hypothesis that, unlike Li_2MnO_3 and Li_2TiO_3, Li_2ZrO_3 does not form a composite structure with $LiMn_{0.5}Ni_{0.5}O_2$ and, therefore, that the Li_2ZrO_3 component does not interfere with the electrochemical operation of the active $LiMn_{0.5}Ni_{0.5}O_2$ species, particularly in

(39) Shao-Horn, Y.; Hackney, S. A.; Armstrong, A. R.; Bruce, P. G.; Gitzendanner, R.; Johnson, C. S.; Thackeray, M. M. *J. Electrochem. Soc.* **1999**, *146*, 2404.

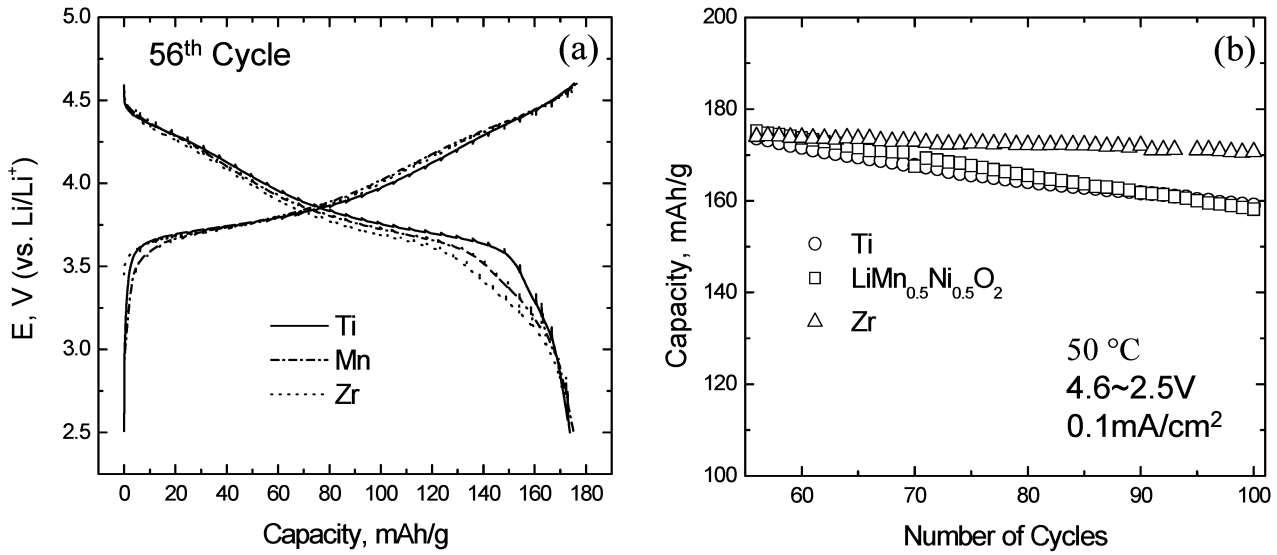

Figure 7. Voltage profiles (a) and capacity vs cycle number plots (b) of Li/0.03$Li_2M'O_3$·0.97$LiMn_{0.5}Ni_{0.5}O_2$ cells (M′ = Mn, Ti, Zr) between 4.6 and 2.5 V at 50 °C. (Cells were cycled at room temperature to the 55th cycle.)

the formation of the $Li_2Mn_{0.5}Ni_{0.5}O_2$ structure at potentials below 2.0 V. By contrast, the 0.03Li_2TiO_3·0.97$LiMn_{0.5}Ni_{0.5}O_2$ electrode shows greater polarization, reaching the voltage limits during charge (4.6 V) and discharge (1.45 V) more rapidly than the 0.03Li_2MnO_3·0.97$LiMn_{0.5}Ni_{0.5}O_2$ and 0.03Li_2ZrO_3·0.97$LiMn_{0.5}Ni_{0.5}O_2$ electrodes (Figure 6a). Consequently, the 0.03Li_2TiO_3·0.97$LiMn_{0.5}Ni_{0.5}O_2$ electrode delivers a lower capacity over this range (∼180 mA·h/g) compared to the equivalent Li_2MnO_3- and Li_2ZrO_3-component systems (300−225 mA·h/g; Figure 6b). Nevertheless, despite its inferior capacity, the 0.03Li_2TiO_3·0.97$LiMn_{0.5}Ni_{0.5}O_2$ electrode cycles with greater stability and efficiency than the Li_2MnO_3- and Li_2ZrO_3-based electrodes. Higher capacity can be achieved from 0.03Li_2TiO_3·0.97$LiMn_{0.5}Ni_{0.5}O_2$ electrodes by lowering the voltage limit to 1.25 V (or by decreasing the current) to access the Li_2MO_2 structure, as reported in an earlier paper.[12]

When 0.03$Li_2M'O_3$·0.97$LiMn_{0.5}Ni_{0.5}O_2$ electrodes (M = Mn, Ti, Zr) cells are cycled at 50 °C over the high-potential region (4.6−2.5 V) alone, the Li_2ZrO_3-based electrode provides excellent cycling stability, whereas the Li_2MnO_3- and Li_2TiO_3-based electrodes lose capacity at an almost identical rate (Figure 7a,b). The superior performance obtained from 0.03Li_2ZrO_3·0.97$LiMn_{0.5}Ni_{0.5}O_2$ electrodes is similar to that obtained from ZrO_2-coated $LiMn_{0.5}Ni_{0.5}O_2$ electrodes and is further evidence that the Li_2ZrO_3 component is not integrated into the $LiMn_{0.5}Ni_{0.5}O_2$ electrode in the same way as the Li_2MnO_3 and Li_2TiO_3 components are, but rather that it may act independently, like ZrO_2, to scavenge H_2O and HF components in the cell to improve electrochemical performance.[40]

The voltage profiles and cycling behavior of Li/0.30$Li_2M'O_3$·0.70$LiMn_{0.5}Ni_{0.5}O_2$ cells for M′ = Mn and Ti between 4.6 and 1.45 V are shown in parts a and b, respectively, of Figure 8. (X-ray diffraction showed that it was not possible to synthesize a corresponding 0.30Li_2ZrO_3·0.70$LiMn_{0.5}Ni_{0.5}O_2$ product.) The 0.30Li_2TiO_3·0.70$LiMn_{0.5}Ni_{0.5}O_2$ electrode performs in much the same way as 0.03Li_2TiO_3·0.97$LiMn_{0.5}Ni_{0.5}O_2$, but yields significantly lower capacities over both high-voltage and low-voltage regions, indicating the electrochemical inactivity of the Li_2TiO_3 component. By contrast, the 0.30Li_2MnO_3·0.70$LiMn_{0.5}Ni_{0.5}O_2$ electrode yields a significantly higher capacity. In this case, electrochemical activity is apparently induced into the Li_2MnO_3 component when cells are charged to 4.6 V. Of particular significance is the difference in the shape of the voltage profiles during the first and second charge of the Li/0.30Li_2MnO_3·0.70$LiMn_{0.5}Ni_{0.5}O_2$ cells and the increase in charging capacity that is obtained on the second cycle. These observations are consistent with the data reported by Dahn et al.[17] in their studies of the analogous $Li[Ni_xLi_{(1/3-2x/3)}Mn_{(2/3-x/3)}]O_2$ system ($0 < x < 0.5$).

It has been previously demonstrated that electrochemical activity can be induced into Li_2MnO_3 either chemically, by acid treatment,[1,2] or electrochemically.[19] Acid treatment using concentrated H_2SO_4 (a dehydrating agent) is accompanied first by an ion-exchange reaction to yield $Li_{2-x}H_xMnO_3$ (alternatively, $H[Li_{0.33}Mn_{0.67}]O_2$, which at $x = 1.5$ is isostructural with $HCrO_2$) and, thereafter, by the removal of the H_2O and Li_2O components from $Li_{2-x}H_xMnO_3$ (which at $x = 1.5$ can be defined, in component form, as 0.25Li_2O·0.75H_2O·MnO_2) to yield a layered MnO_2 type structure. The Mn and some residual Li^+ ions occupy octahedral sites in the Mn^{4+} layers, whereas residual protons are H-bonded to oxygen atoms in alternate layers.[18] Note that, in the ideal case, when the Li_2O component is completely removed from Li_2MnO_3 (alternatively, Li_2O·MnO_2), two Li^+ ions are removed for every O^{2-} ion to yield MnO_2. Therefore, the gradual removal of Li_2O from Li_2MnO_3 (as $Li_{2-x}MnO_{3-x/2}$ for $0 < x < 1$) creates interstitial sites for lithium, which induces electrochemical activity and capacity into the $Li_{2-x}MnO_{3-x/2}$ structure. These arguments have been used previously to explain the electrochemical activity of acid-leached Li_2MnO_3 samples.[1,18] Li_2MnO_3 can also be activated directly by electrochemical methods in lithium cells;[19] in this case, it has been proposed that the electrochemical activity is achieved

(40) Thackeray, M. M.; Johnson, C. S.; Kim, J.-S.; Lauzze, K. C.; Vaughey, J. T.; Dietz, N.; Abraham, D.; Hackney, S. A.; Zeltner, W.; Anderson, M. A. *Electrochem. Commun.* **2003**, *5*, 752.

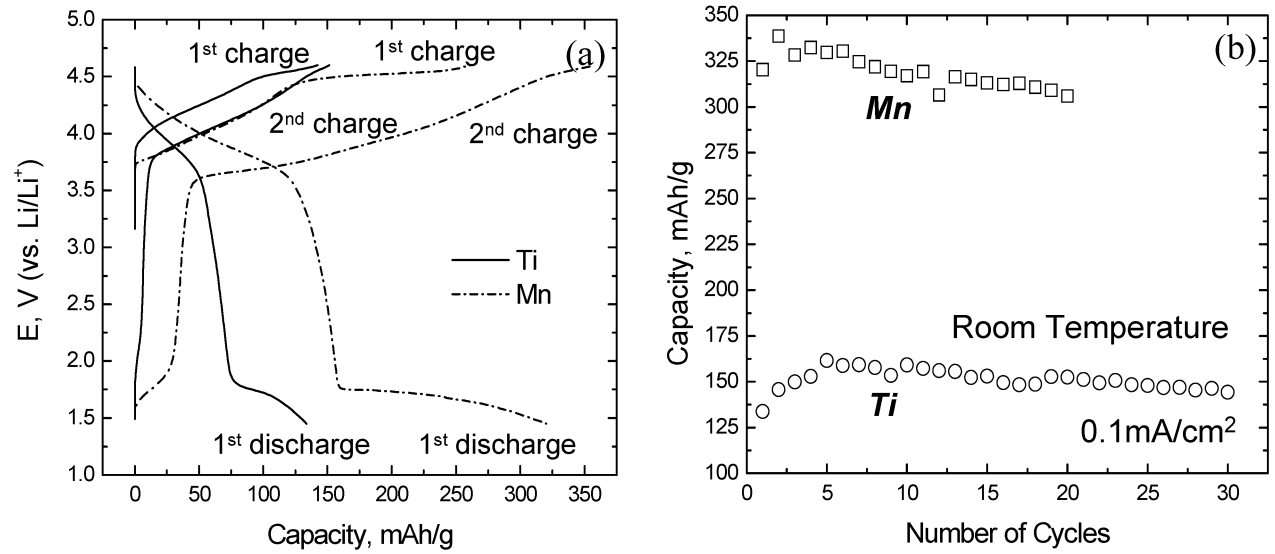

Figure 8. Voltage profiles (a) and capacity vs cycle number plots (b) of $Li/0.30Li_2M'O_3\cdot0.70LiMn_{0.5}Ni_{0.5}O_2$ cells (M′ = Mn, Ti) between 4.60 and 1.45 V at room temperature.

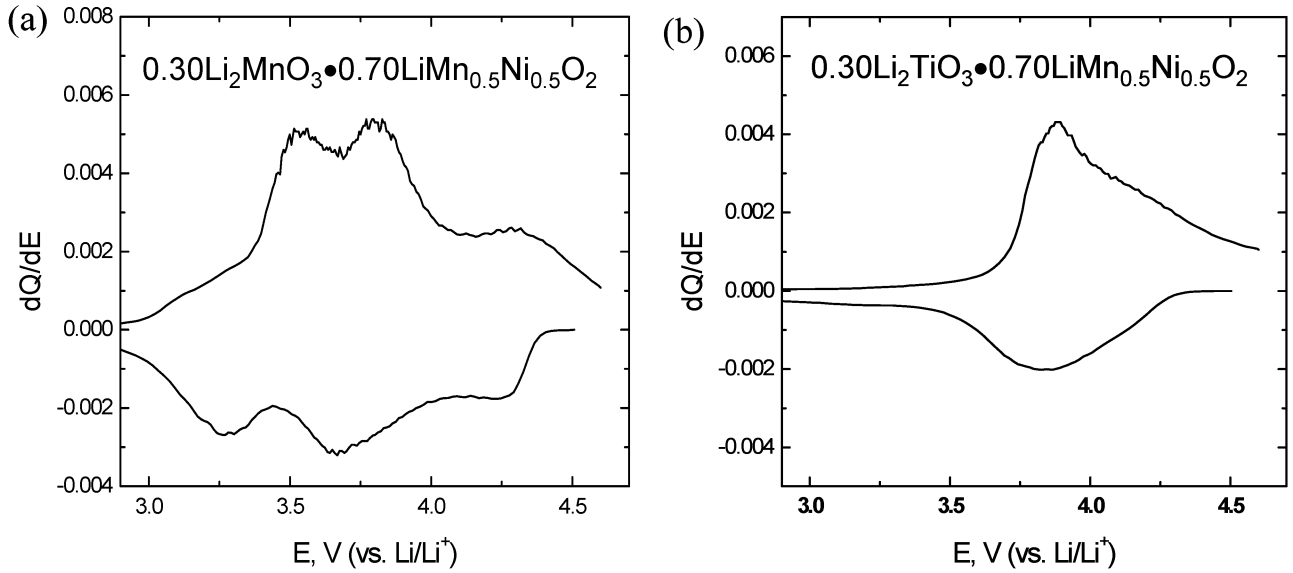

Figure 9. dQ/dE plots of the 15th cycle of $Li/0.30Li_2M'O_3\cdot0.70LiMn_{0.5}Ni_{0.5}O_2$ cells cycled between 4.60 and 2.5 V: (a) M′ = Mn; (b) M′ = Ti.

by a proton-exchange mechanism, similar to that described above, with the protons being derived from the electrolyte medium in the cells. With this information, it is perhaps not surprising that high electrochemical capacities can be derived from composite $xLi_2MnO_3\cdot(1-x)LiMn_{0.5}Ni_{0.5}O_2$ electrodes, even those with a high Li_2MnO_3 content (e.g., $x = 0.3$), as shown in Figure 8.

We interpret the very high rechargeable capacity (>300 mA·h/g) that can be obtained from $0.30Li_2MnO_3\cdot0.70LiMn_{0.5}Ni_{0.5}O_2$ composite electrodes when charged and discharged between 4.6 and 1.45 V, as follows. (Note that if the Li_2MnO_3 component is considered electrochemically inactive and if the compositional range of the $Li_xMn_{0.5}Ni_{0.5}O_2$ component is $0 \le x \le 2$, a $0.3Li_2MnO_3\cdot0.7LiMn_{0.5}Ni_{0.5}O_2$ electrode would provide a theoretical capacity of 368 mA·h/g.) In the absence of detailed structural information on the composite electrodes, in particular the cation distribution in the transition-metal layers, we use the Li_2MnO_3 composition and structure to simplify the discussion. The theoretical capacity of a $0.30Li_2MnO_3\cdot0.70LiMn_{0.5}Ni_{0.5}O_2$ electrode corresponding to complete extraction of lithium from the $LiMn_{0.5}Ni_{0.5}O_2$ component is 184 mA·h/g. However, the capacity derived from this electrode when initially charged to 4.6 V is 260 mA·h/g, that is, significantly more than the theoretical capacity of the electrode. Our data are in agreement with Dahn et al.'s[17] results from the analogous $Li[Ni_xLi_{(1/3-2x/3)}Mn_{(2/3-x/3)}]O_2$ system. However, we believe that, in these $xLi_2MnO_3\cdot(1-x)LiMn_{0.5}Ni_{0.5}O_2$ composite electrodes, the electrochemical activity is induced during the initial charge of the cell predominantly by removal of lithium (as Li_2O) from the Li_2MnO_3 component at ~4.5 V vs Li^0 (as also implied by Dahn et al.[17]) rather than by a H^+ ion-exchange mechanism and the electrolysis of a H_2O component, which has been suggested for the compound $Li_{2-x}H_xMnO_3$ ($x \approx 1.5$, alternatively $H[Li_{0.33}Mn_{0.67}]O_2$),[18] because the acid concentration in commonly used lithium battery electrolytes is low. We also support the hypothesis that electrochemical removal of Li_2O from the

structure occurs via an intermediate process at the electrode surface whereby lithium extraction from the Li_2MnO_3 component is accompanied by removal of electrons from the oxygen 2p band, leaving an unstable oxidized surface behind, which is consequently stabilized by the loss of oxygen. This electrochemical process at the surface of the Li_2MnO_3 component can be represented by the following reaction sequence,

$$Li_2MnO_3 \rightarrow 2Li^+ + Mn^{4+}O_3^{4-} + 2e^- \quad \textit{electrochemical process} \quad (1)$$

during which electrons are removed from the oxygen 2p band to form an unstable $Mn^{4+}O_3^{4-}$ intermediate configuration, followed by an immediate chemical redox reaction to stabilize the electrode surface by loss of oxygen either as a gas or by reaction with the electrolyte:

$$2Mn^{4+}O_3^{4-} \rightarrow 2MnO_2 + O_2 \quad \textit{chemical process} \quad (2)$$

The formation of a MnO_2 species, which remains structurally integrated at the surface of layered $xLi_2MnO_3 \cdot (1-x)LiMn_{0.5}Ni_{0.5}O_2$ composite electrodes during the initial charge, is consistent with the high capacities that have been obtained from the electrodes on subsequent charge/discharge cycles at both high (4.6−2.5 V) and low potentials (2.5−1.45 V) (Figure 8).

It has been established that when $LiMn_{0.5}Ni_{0.5}O_2$ electrodes are cycled between 4.2 and 3.0 V, the predominant reaction occurs by electron transfer between Ni^{2+} and Ni^{4+} ions and that the Mn^{4+} ions are electrochemically inactive. However, increasing the MnO_2 content in $xLi_2MnO_3 \cdot (1-x)LiMn_{0.5}Ni_{0.5}O_2$ electrodes during an initial charge to 4.6 V introduces Mn^{4+}/Mn^{3+} character to the electrode, as shown by the reversible process that occurs at approximately 3.25 V (during discharge) in the dQ/dE plot of a $0.30Li_2MnO_3 \cdot 0.70LiMn_{0.5}Ni_{0.5}O_2$ electrode after 15 cycles (Figure 9a). By contrast, the $0.30Li_2TiO_3 \cdot 0.70LiMn_{0.5}Ni_{0.5}O_2$ shows no such response (Figure 9b), thereby confirming the electrochemical inactivity of the Li_2TiO_3 component in the high-potential range.

Finally, the high capacity and excellent rechargeability of $xLi_2MnO_3 \cdot (1-x)LiMn_{0.5}Ni_{0.5}O_2$ composite electrodes at low potentials between 2.0 and 1.45 V, even those with high Li_2MnO_3 content (e.g., $x = 0.3$), reflects an ability of these composite structures to form layered $Li_2Mn_{1-x}Ni_xO_2$-type structures in which x may vary over a wide range. Perhaps this is not surprising given the fact that both Li_2MnO_2[30] and Li_2NiO_2[31] have already been shown to exist as independent compounds.

Conclusions

Layered $Li_2M'O_3$ compounds, such as Li_2MnO_3 and Li_2TiO_3, can be structurally integrated into $LiMn_{0.5}Ni_{0.5}O_2$ to yield composite electrode materials $xLi_2M'O_3 \cdot (1-x)LiMn_{0.5}Ni_{0.5}O_2$ for $0 < x \leq 0.3$. HRTEM images, supported by MAS NMR data, provide evidence that the cations in the transition-metal layers are not homogeneously distributed as a solid solution, but are rather distributed in an irregular manner in domains with short-range order. Electrochemical data obtained in lithium cells between 4.6 and 1.45 V shows that the Li_2TiO_3 component remains electrochemically inactive during charge and discharge. It appears that Li_2ZrO_3 does not integrate structurally with $LiMn_{0.5}Ni_{0.5}O_2$ and may act independently to scavenge H_2O and HF from the electrolyte. By contrast, electrochemical activity can be induced into the Li_2MnO_3 component of a $xLi_2MnO_3 \cdot (1-x)LiMn_{0.5}Ni_{0.5}O_2$ structure, which is consistent with data reported previously for pure Li_2MnO_3 electrodes. The high rechargeable capacity (~300 mA·h/g) obtained from a $0.3Li_2MnO_3 \cdot 0.7LiMn_{0.5}Ni_{0.5}O_2$ electrode between 4.6 and 1.45 V was attributed to the loss of Li_2O from the Li_2MnO_3 component electrode above 4.3 V and to the generation of a Li_2MO_2-type structure below 2 V.

Acknowledgment. Financial support from the Office of Basic Energy Sciences (for the HRTEM experiments) and the Office of FreedomCar and Vehicle Technologies of the U.S. Department of Energy (for the electrochemical and NMR experiments) under Contract No. W31-109-Eng-38 and DE-AC03-76SF00098 subcontract no. 6517749 is gratefully acknowledged.

CM0306461